

CNS MR and CT Findings Associated with a Clinical Presentation of Herpetic Acute Retinal Necrosis and Herpetic Retrobulbar Optic Neuritis: Five HIV-Infected and One Non-Infected Patients

Robert J. Bert, Ranji Samawareerwa, and Elias R. Melhem

INTRODUCTION: This report demonstrates the spectrum of central nervous system (CNS) abnormalities observed on MR imaging and CT studies in 6 patients with clinical or pathologic diagnoses of acute retinal necrosis (ARN) and retrobulbar optic neuritis (RBON-H) resulting from Herpes Zoster Virus and Cytomegalovirus. We discuss the etiologic and pathophysiologic implications regarding these findings.

METHODS: Standard MR imaging sequences of the whole brain and selected high-resolution images of the orbits and globes, from 6 patients, were reviewed by three neuroradiologists for consensus interpretation of the findings. Special sequences augmenting disease were obtained in individual cases. Axial CT images were obtained from two patients using 5mm sequential slices.

RESULTS: MR imaging findings showed both T2 signal brightening and contrast enhancement in one or both optic nerves, optic tracts and lateral geniculate bodies, as well as the postsynaptic optic radiations and optic cortex. Similar findings were observed in the superior colliculus, lateral midbrain and cerebellum, with multiple potential etiologic possibilities regarding pathways of dissemination. Low T2* signal (indicating magnetic field susceptibility effects) and CT hyperdensity, consistent with prior hemorrhage, were also observed in the optic tracts, optic radiations and lateral geniculate bodies. Post-contrast enhancement was observed in the meninges and Meckle's cave in one HIV negative patient.

CONCLUSION: These cases demonstrate CNS imaging findings associated with RBON that are temporally-related to ARN. They support the hypothesis that RBON can either precede or follow ARN and implicate transneuronal, transsynaptic and/or transcerebrospinal fluid viral spread by the herpetic family.

Acute retinal necrosis (ARN) and retrobulbar optic neuritis of herpetic origin (RBON-H) are diseases usually seen in severely immunocompromised patients (with CD4 counts typically below 20%), such as those with HIV infection (1–4). In the immunocompromised population, members of the *Herpesviridae* family are usually found as etiologic agents. Most typically, the specific viruses are herpes zoster virus (HZV) or cytomegalovirus (CMV), but herpes sim-

plex virus 1 is occasionally involved (5, 6). Both ARN and RBON-H secondary to these viruses are rapidly progressive in untreated patients, and they typically lead to blindness that can be bilateral (7–9). ARN attributable to HZV or CMV can often be distinguished clinically. HZV can produce progressive outer retinal necrosis (5, 10, 11), which is clinically distinguishable from the hemorrhagic retinitis produced by CMV (12–17). The different pathogens, however, may coexist (5). It has not been possible to distinguish CMV from HZV infections causing RBON-H.

On the basis of case reports and small series, some have hypothesized that ARN and RBON-H are etiologically related (7–9, 18–20). Some authors have proposed that ARN can spread in antegrade fashion to produce RBON-H (18, 19), while others have pro-

Received October 23, 2002; accepted after revision January 28, 2004.

From the Boston Medical Center (R.J.B., E.R.M.) and the Boston VA Medical Center, Jamaica Plain (R.S.), MA.

Address reprint requests to Robert J. Bert, MD, PhD, Department of Radiology, New England Medical Center, 750 Washington Street, Boston, MA 02131.

posed that RBON-H might serve as a precursor to ARN (7, 8, 20). Furthermore, herpes ophthalmicus has preceded both ARN and RBON-H (7, 9, 21). CT scanning and MR imaging findings are rarely reported in the small clinical series presented to date. In reviewing the literature, we observed relatively few cases that described the imaging findings (22–24), with some cases reporting an absence of findings (7, 8).

In this review, we describe a series of MR imaging and CT studies in six patients with clinical diagnoses of ARN and RBON-H associated with the *Herpesviridae* (HZV in four, HZV and CMV in two). In the cases involving HZV, three were established by unequivocal clinical findings. In one case, pathologic evidence of HZV infection was obtained on autopsy. The two cases of CMV retinitis were established clinically. We believe that the imaging findings in these cases have important implications on the etiology and pathophysiology of these disorders. Implications of the relationship between ARN and RBON-H, including possible trans-synaptic viral spread, are discussed.

Methods

Three neuroradiologists (R.J.B., R.S., E.R.M.) reviewed standard MR images of the whole brain and selected high-resolution images of the orbits and globes from the six patients. Imaging with special sequences to augment pathologic analysis was performed in individual cases. In two patients, axial CT scans were obtained by using 5-mm sequential sections.

MR Imaging

Multiple sequences were performed in five patients by using one of two 1.5-T magnets (Philips Imaging Systems; GE Medical Systems, Milwaukee, WI). The following whole-brain sequences were applied in all patients: 1) nonenhanced and gadolinium-enhanced axial T1-weighted sequence (TR/TE = 400/40, in-plane resolution of $500 \times 500 \mu\text{m}$, number of patients [n] = 4); 2) axial T2-weighted, turbo spin-echo sequence (Philips Imaging Systems, 2000/200, n = 5) and sagittal T1-weighted spin-echo sequence (400/40, in-plane resolution of $500 \times 500 \mu\text{m}$, number of patients [n] = 3); 3) axial T2-weighted fluid-attenuated inversion recovery sequence (FLAIR, TR/TE/TI = 2000/200/180, n = 3); and 4) gadolinium-enhanced axial T2-weighted FLAIR sequence (2000/200/180 ms, n = 1). For all of these sequences, a matrix of 256×256 , 5-mm section thickness, and 0.5-mm gap were used.

Orbital or optic nerve high-resolution images were obtained in four patients by using the following: 1) nonenhanced and gadolinium-enhanced coronal and axial T1-weighted, turbo spin-echo sequence with chemical fat saturation (SPIR; Philips Imaging Systems [400/40, in-plane resolution of $250 \times 250 \mu\text{m}$, n = 3]); 2) axial high-resolution, T2-weighted FLAIR turbo spin-echo sequence with chemical fat saturation (SPIR; Philips Imaging Systems [400/40, in-plane resolution of $250 \times 250 \mu\text{m}$, n = 1]); and 3) sagittal spin-echo T2-weighted sequence (2000/200, 0.3-mm gap). For all of these sequences, a matrix of 256×256 and 3-mm section thickness were used.

CT Scanning

Axial CT scans were obtained in two patients by using 5-mm sequential scans throughout the brain (GE Medical Systems, 24-cm field of view, 130 kV, 175 mA, 525 mAs, half compensation).

Clinical Courses

Pertinent clinical findings from the six cases are summarized in Table 1. Typical examples of the clinical course in a patient with HIV (case 3) and the clinical presentation from the one patient without immunodeficiency disease (case 6) in our series are presented.

Case 3.—A 38-year-old homosexual white man was seropositive for HIV and presented with HZV infection in the T8 dermatome in June 1991. His medical history included a fracture of the cervical spine and shoulder dislocation but was otherwise unremarkable. His helper inducer T-lymphocyte (CD4) count at presentation was 80 (8%). Zidovudine was started for HIV treatment, and trimethoprim-sulfamethoxazole was given as prophylaxis for *Pneumocystis carinii* pneumonia (PCP). The patient's CD4 count continued to decline, and didanosine was added to his treatment in June 1992. In May 1993, he developed *Candida* esophagitis, which was treated with fluconazole. In November 1993, he developed recurrent HZV infection in the T6 dermatome. At this time, his CD4 count had decreased to 5 (1%). Despite the HZV infection, acyclovir was not used.

In November 1994, the patient developed a foreign-body sensation and photophobia in the left eye. Ophthalmologic examination revealed dendritiform lesions arising in the limbus, and his visual acuity was 20/20 in both eyes. Herpes simplex keratitis was diagnosed, and treatment was begun with topical acyclovir and steroids in both eyes. Findings from follow-up retinal examination were unremarkable for both eyes. A week later, examination revealed deterioration, with 20/300 visual acuity in the right eye and evidence of progressive outer retinal necrosis in both eyes, much more in the right eye than in the left. At this time, intravenous ganciclovir and acyclovir were started. Because the patient's WBC count continued to decrease, an intraocular ganciclovir implant was placed in the left eye in mid-December. However, progressive outer retinal necrosis progressed further; therefore, intravenous foscarnet and open-label BV-AraU (Serivudine; Bristol-Myers-Squibb, New York, NY) were initiated. His condition slowly improved over the next 2 months.

In March 1995, he presented with paresthesias of the left lower extremity, gait ataxia, and slurred speech. CT scanning and MR imaging (of partially limited quality) demonstrated an enhancing mass lesion in the posterior limb of the internal capsule. Toxoplasmosis was the presumed diagnosis, and sulfadiazine and pyrimethamine were initiated. Follow-up MR imaging revealed multiple areas of enhancement in the right internal capsule, thalamus, occipital cortex, and upper right side of the midbrain. Retinal examination showed no lesions owing to active progressive outer retinal necrosis at this time. CSF examination revealed one RBC, three lymphocytes, a protein level of 59 mg/dL, and a glucose level of 54 mg/dL. Blood, urine, and CSF cultures were negative. CNS lymphoma was suspected; thallium scans of the brain were negative. Foscarnet was discontinued, but BV-AraU and acyclovir were continued. At this time, biopsy was recommended but declined by family, and hospice care was begun. Treatment for the possibility of lymphoma was initiated with dexamethasone. However, because of the patient's clinical deterioration, the steroid was discontinued 1 week later. Analysis of aspirated vitreous fluid was positive for HZV, and immunofluorescent staining at autopsy revealed HZV in the brain lesions.

Case 6.—An 82-year-old woman was brought to a Boston-area hospital after 4 days of weakness and decreased oral intake. She described a rash on her left forehead, which started 2 weeks earlier, with associated periorbital and eyelid swelling but no paresthesias or dermatomal pain. She complained of a headache but denied neck stiffness, fever, chills, cough, chest pain, shortness of breath, and abdominal pain. She had been examined in an outpatient clinic 4 days before this presentation, and oral acyclovir had been started. Her medical history included subtotal thyroidectomy, multiple urinary tract infec-

TABLE 1: Clinical findings

Patient	HIV Status	CD4 Count (%)	WBC Count (k/ μ l)	Retinal Diagnosis	Onset		Vision			Lumbar Puncture
					ARN	RBON-H or CNS Infection	OD	OS	OS	
1	Positive	Normal*	Low†	CMV ARN, OS>OD	Feb-Mar 1988	July 1988	Decreased to blind	Moderately to severely decreased	NO	NO
2	Positive	12	Low†	CMV ARN, OU	Mar 1994	Mar 1994	Severely decreased	Severely decreased	NO	NO
3	Positive	5-80	Low†	HZV progressive ORN, OS>>OD	Nov 1994	Mar 1995	20/300	20/20, later decreased	Normal	Normal
4	Positive	30	2.2	HZV progressive ORN, OD>>OS	Aug 1998	Aug 1998	Blind	20/60	NO	NO
5	Positive	3-44	11	HZV progressive ORN, CMV OS	Mar, Aug 1998	Mar 1998	Blind	24/100	Normal	Normal
6	Negative	Normal	4.6	Normal	Normal	Sept 1929	Iritis, decreased	Iritis, decreased	HZV, positive	WBC count‡, increased

Note.—OD indicates oculus dexter (right eye); ORN, outer retinal necrosis; OS, oculus sinister (left eye); NO, not obtained.

* T4/T8 ratio of 126/16, used for prognosis prior to the establishment of CD4 subtypes.

† WBC count was recorded only as "below normal" in the obtainable records.

‡ Lumbar puncture was traumatic, and samples grew skin contaminants after 3 days.

tions, degenerative joint disease, a positive purified protein derivative result for tuberculosis (which was treated with isothioniazide in 1974), chronic obstructive pulmonary disease, left bundle branch block, anemia, and anxiety. Her usual medication regimen consisted of alendronate sodium, ibuprofen, senna (Senokot; Purdue Pharma L.P., Stamford, CT), triamterene (Dyazide; SmithKline Beecham, Philadelphia, PA) and polysaccharide-iron complex (Niferex; Thera-Rx Corp., St. Louis, MO).

Her routine admitting examination revealed the following: blood pressure of 149/80 mm Hg, heart rate of 84 beats per minute, oral temperature of 74.8°F, clear lungs, extra S4 heart sounds and systolic ejection murmur with an increased point of maximum impulse, and normal abdominal findings. Skin lesions were noted in the fifth cranial nerve (V1-V2) area; these were crusted and golden-brown in color. Associated swelling of the left eyelid was observed. Neurologic examination showed normal cranial nerves V-XII, decreased alertness, and an unsteady gait. Ophthalmic examination showed enlarged pupils that were minimally reactive, and slitlamp examination showed conductive iritis with pseudodendrites but no uveitis or retinitis. Laboratory workup indicated a WBC count of 4.6 k/ μ l, a hematocrit value of 36%, a platelet count of 165 k/ μ l, an international normalized ratio of 1.2, and normal electrolyte and glucose levels. The chest radiograph and electrocardiogram obtained on admission showed clear lungs and a left bundle branch block, respectively.

On admission, the patient's treatment with oral acyclovir was continued, and neurotonin was started to treat herpetic neuralgia. Throughout the first day of her admission, the patient's mental status waxed and waned. This was initially attributed to an underlying mild dementia exacerbated by her hospitalization, which had placed the patient in an unfamiliar environment. During this first day, oral acyclovir was changed to an intravenous dose of 7.5 mg/kg. Topical erythromycin ointment was added to her skincare regimen to prevent superinfection.

Despite this initial management, the patient's mental status continued to decline, with increased confusion and visual hallucinations noted over the next 24-48 hours. Additional laboratory tests were performed to check her vitamin B12, thyroid stimulating hormone, and rapid plasma reagent (RPR) levels; all were normal. After her mental status continued to decline, herpes encephalitis was suspected and MR imaging was ordered. T1-weighted images showed contrast enhancement of the Meckle cave with associated faint enhancement of the pons, midbrain, optic chiasm, and tentorium cerebelli. Inversion recovery images showed faintly increased T2 signal intensity in the same tissues. Contrast enhancement was more clearly demonstrated on contrast-enhanced T2-weighted FLAIR images and on T1-weighted images with a magnetization transfer pulse applied. The findings were reported as being consistent with CNS spread of HZV ophthalmicus. Lumbar tap was performed and showed: 489 WBCs (31% polymorpholeukocytes), 21 mononuclear cells, and elevated protein and normal glucose levels. Results of polymerized chain reaction (PCR) testing for varicella-zoster virus were positive.

The patient's clinical course consisted of continued mental status decline during the third day; this was attributed to an aspiration pneumonia, as demonstrated by bilateral infiltrates on follow-up chest radiographs, decreased oxygen saturation, and a newly elevated WBC count. Intravenous antibiotics (ceftriaxone and clindamycin) were started, with eventual improvement. Her recovery was further complicated by the development of syndrome of inappropriate antidiuretic hormone (SIADH) secretion, as diagnosed on the basis of a depressed serum sodium level (119 mg/dL) with an elevated urine sodium level (120 mg/dL). SIADH was attributed to the HZV meningocerebritis. Water restriction and diuresis with lasix was started, with subsequent slow improvement. The patient's status continued to improve, and she was discharged home in

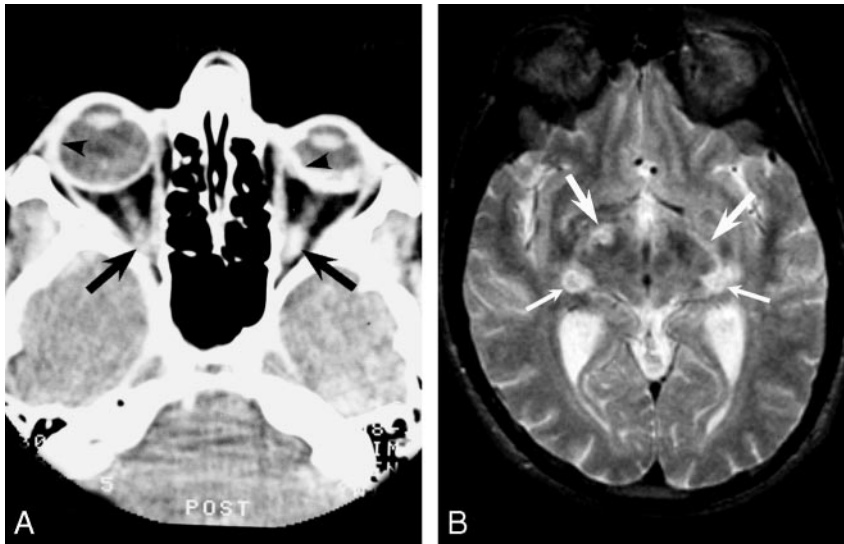


FIG 1. Images from 1988 obtained in a patient with AIDS with CMV-induced ARN preceding retrobulbar optic neuritis.

A, CT scan shows a shrunken left globe with bilateral avidly enhancing sclera (arrowheads) and enhancement of both optic nerves (arrows).

B, T2-weighted image shows increased signal intensity in the optic tracts (top arrows) and geniculate bodies (bottom arrows).

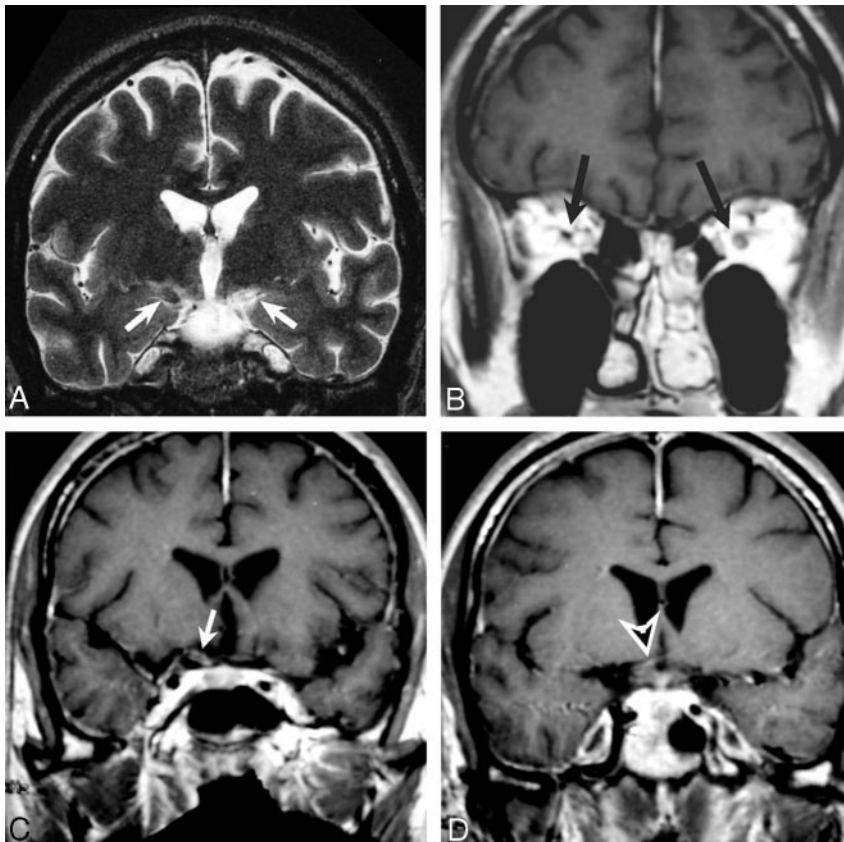


FIG 2. MR images obtained in patient 2. A, T2-weighted coronal image shows both increased (left) and decreased (right) signal in the optic tracts (arrows).

B, Contrast-enhanced T1-weighted image shows enhancement of the left optic nerve and low signal intensity in the right optic nerve (arrows).

C and D, Contrast-enhanced T1-weighted images show enhancement of the right optic tract (arrow in C) and chiasm (arrowhead in D).

October 1999 with cefodoxime and Flagyl (metronidazole; Rhodia, Cranbury, NJ) after completing the course of intravenous acyclovir.

Imaging Findings

Figures 1–5 show the imaging findings from five of the six cases. One case was omitted because the findings were repetitive of those of the other cases. Table 2 summarizes the findings.

CT Findings.—CT examinations were performed in four of the six patients. On nonenhanced CT scans, hypoattenuating changes occurred along the optic tracts in two of the

four patients (patients 3 and 6). These two patients had diagnoses of HZV, one of which was established clinically and the other, pathologically. Hyperattenuation was seen along the optic tracts of another patient, patient 2. Contrast-enhanced CT series were obtained for a single patient (patient 1) and enhancement was seen in both optic nerves, both retinas, and both sclerae (Fig 1). These hyperattenuating lesions accompanied mixed low and high signal intensity in the optic tracts and geniculate bodies on a T2-weighted MR image in the same patient (Fig 1). The destruction induced by the infection led to a shrunken left globe (phthisis bulbi), which was also seen in two additional patients (patients 2 and 5).

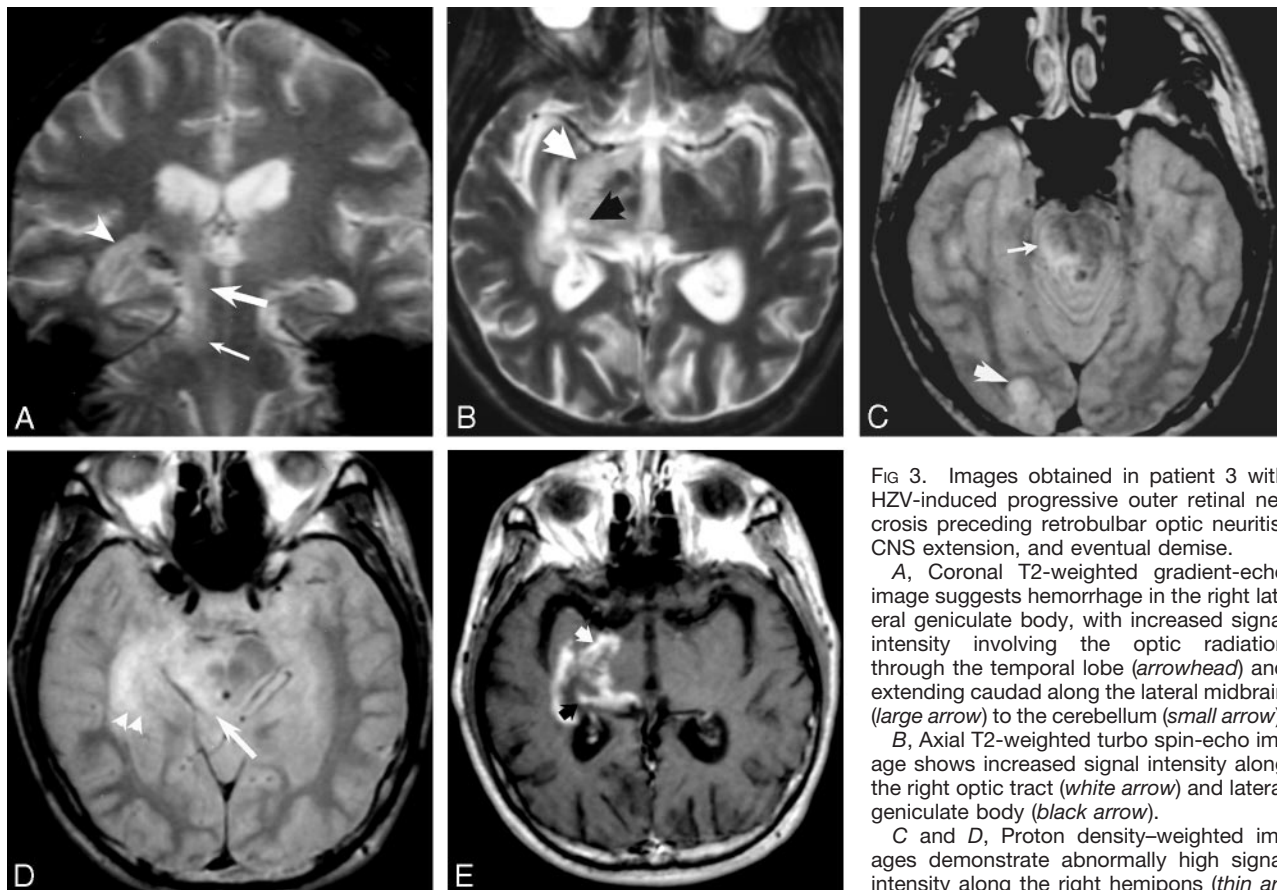


FIG 3. Images obtained in patient 3 with HZV-induced progressive outer retinal necrosis preceding retrobulbar optic neuritis, CNS extension, and eventual demise.

A, Coronal T2-weighted gradient-echo image suggests hemorrhage in the right lateral geniculate body, with increased signal intensity involving the optic radiation through the temporal lobe (*arrowheads*) and extending caudad along the lateral midbrain (*large arrow*) to the cerebellum (*small arrow*).

B, Axial T2-weighted turbo spin-echo image shows increased signal intensity along the right optic tract (*white arrow*) and lateral geniculate body (*black arrow*).

C and D, Proton density-weighted images demonstrate abnormally high signal intensity along the right hemipons (*thin arrow* in C), right midbrain, and superior colliculus (*arrow* in D), occipital (visual) cortex (*thick arrow* in C), and optic radiation in the temporal lobe (*arrowheads* in D).

E, T1-weighted contrast-enhanced image shows contrast enhancement in similar regions: optic tract (*white arrow*) and lateral geniculate body (*black arrow*). Postmortem immunofluorescence stains (not shown) demonstrated HZV in these areas.

MR Imaging Findings.—MR imaging was performed in all six patients. Relative increased T2 signal intensity in the optic pathway was the most consistent finding; this was observed in all patients from whom MR images were available (Figs 1–5). The following structures showed increased T2 signal intensity (Table 2): optic nerves (patients 1, 2, 4–6), optic chiasm (patients 2, 4, 5), optic tracts (patients 1, 2, 4, 5), lateral geniculate bodies (patients 1, 3), optic radiations (patient 3), visual cortex (patient 3), midbrain structures (patients 3, 6), trigeminal nerves (patients 3, 6), and meninges (patient 6). Although T2-weighted FLAIR images were obtained in three patients (patients 4–6), meningeal changes were visible on FLAIR images in only a single study (patient 6). Increased T2 signal intensity in the optic tracts and optic radiations were most conspicuous on the heavily T2-weighted images, whereas the FLAIR images better demonstrated changes in the optic nerves, meninges, and optic chiasm.

Decreased T2* Signal Intensity.—Decreased T2* signal intensity in the optic pathway was seen in two cases (patients 2, 3) (Figs 2 and 3). Lesions with these findings occurred in the optic tracts both unilaterally (patient 3) and bilaterally (patient 2). Similar lesions occurred in one optic nerve (patient 3). Overlapping diagnoses of CMV and HZV infection were made in patient 2, while immunofluorescent labeling confirmed HZV infection in patient 3. The findings were thought to represent hemorrhage or mineralization or both.

Contrast Enhancement.—Contrast enhancement along the visual pathway and meninges was observed on MR images obtained in patients 2–6 (Table 2, Figs 2–5). Contrast-enhanced images were not obtained for patient 1. In studies in which contrast material was administered, enhancement was

seen on T1-weighted images in the optic nerve and optic chiasm (patients 2, 4–6); optic tracts (patients 2–6); optic radiation (patient 3); and semilunar ganglion–Meckle cave, midbrain, and meninges (patients 3, 6). HSV was clinically diagnosed in these five patients, although two (patients 2, 3) had an overlapping diagnosis of CMV retinitis post-contrast.

Standard T1-weighted, magnetization-transfer T1-weighted images, and T2-weighted FLAIR images were obtained in a single patient (patient 6, Fig 5). Conspicuity of the enhancement appeared to be most evident with the contrast-enhanced T2-weighted FLAIR sequence.

Atrophy.—Follow-up MR studies were obtained in four patients (patients 2, 4–6). These images showed atrophy or encephalomalacia in all four cases, regardless of treatment.

Discussion

In this review, we showed images from six patients with clinical or pathologic diagnoses of CNS involvement associated with either HZV or CMV. Clinical diagnoses were established on the basis of characteristic ophthalmoscopic findings, vitreous aspirate results, or classically associated skin lesions. We believe the CT scanning and MR imaging changes represent areas of viral infection and associated inflammation. In one case, this hypothesis was confirmed at autopsy. In the other cases, both symptom onset and post-treatment improvement was correlated with the changes in MR imaging signal intensity. Table 2 sum-



FIG 4. Patient 4 with HZV-induced progressive outer retinal necrosis and retrobulbar optic neuritis after herpes ophthalmicus. T1-weighted contrast-enhanced image shows enhancement of the optic nerves (right distal, left proximal) and optic chiasm (arrows). Compare the thickened, avidly enhancing right chorioretina with the normally enhancing left retina (arrowheads).

marizes the results observed on the CT scanning and MR imaging studies, showing the spectrum of imaging findings that we observed. Imaging findings were seen throughout the visual pathways, including the superior colliculi. Involvement of the meninges, midbrain, and cerebellum were also observed in two cases.

We believe that our findings are consistent with the first two of three possible hypotheses that have been proposed for the dissemination of herpes viruses from the globe or ophthalmic division of the trigeminal nerve to the CNS (28): 1) transneuronal spread from the retina with antegrade, retrograde, and trans-synaptic spread to other visual structures; 2) transneuronal spread from the trigeminal ganglia to its innervations of the meninges, followed by CSF spread to other structures; and 3) transneuronal spread to the vessels of the CNS innervated by the trigeminal nerve, with resulting vasculitis.

Transneuronal and trans-synaptic spread of HSV and other viruses to the CNS has been demonstrated in animal models (25–27). Furthermore, imaging studies have shown associated CNS lesions in cases of peripheral HZV infection of the ear (Ramsey-Hunt syndrome) (29), in cervical dermatomes (spinal cord) (30), and in trigeminal nerve dermatomes (spinal trigeminal nucleus and tract) (31).

Some have also proposed that CNS lesions result from vascular infarcts produced by herpetic spread into vessels innervated by the trigeminal nerve (22–24, 32, 33). Trigeminal projections to the superior

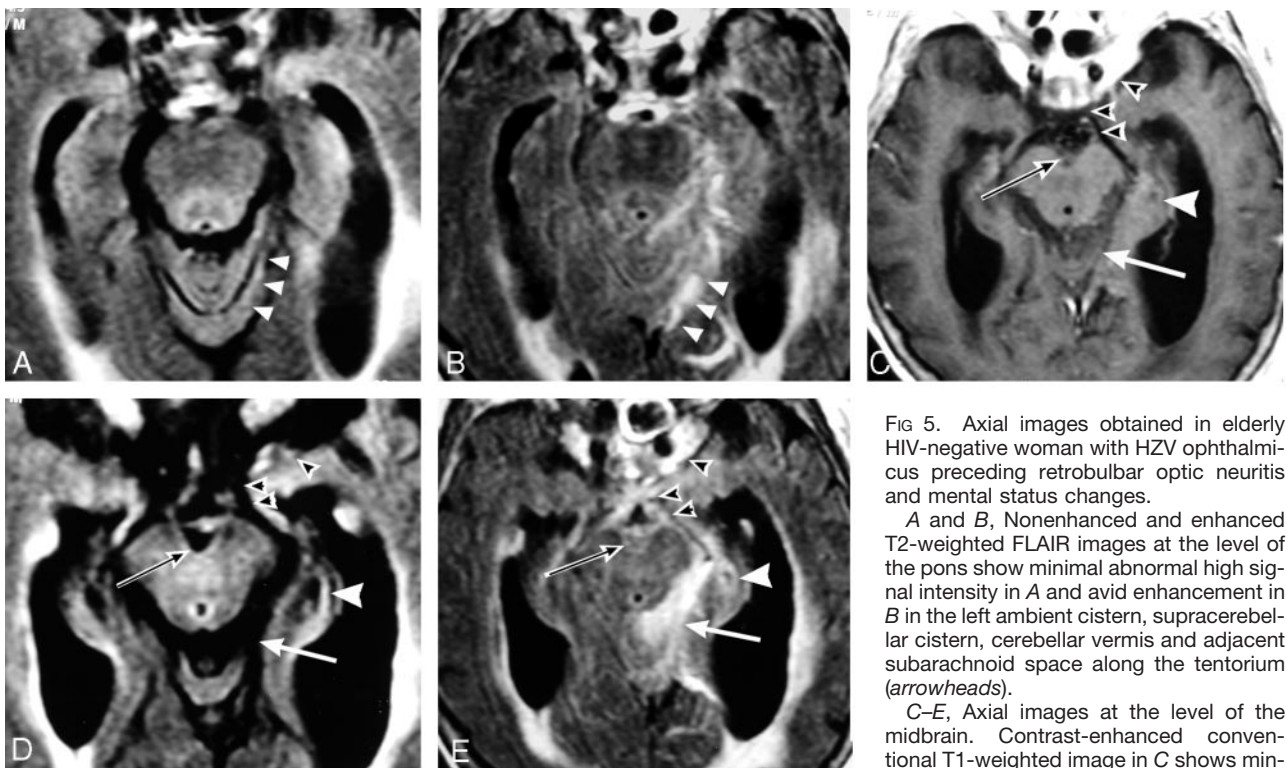


FIG 5. Axial images obtained in elderly HIV-negative woman with HZV ophthalmicus preceding retrobulbar optic neuritis and mental status changes.

A and B, Nonenhanced and enhanced T2-weighted FLAIR images at the level of the pons show minimal abnormal high signal intensity in A and avid enhancement in B in the left ambient cistern, supracerebellar cistern, cerebellar vermis and adjacent subarachnoid space along the tentorium (arrowheads).

C–E, Axial images at the level of the midbrain. Contrast-enhanced conventional T1-weighted image in C shows minimal enhancement. Nonenhanced (D) and

enhanced (E) T2-weighted FLAIR images show avid enhancement of the optic nerves, chiasm, tracts, and pericavernous region (black arrowheads), right lateral geniculate body (white arrowhead), interpeduncular cistern (black arrow), and supracerebellar cistern (white arrow).

TABLE 2: CT and MR imaging findings in six patients with *Herpesviridae* infection and ARN and/or RBON-H

Patient	Optic Nerve	Optic Chiasm	Optic Tract	Lateral Geniculate	Optic Radiation	Visual Cortex
1*	↑ T1, ↑ T2, CECT	↑ T1, ↑ T2	↑ T2	↑ T2	↑ T2	
2	↓ T1, T1E, ↑ T2, HDCT	T1E, ↑ T2	↑ T2, ↓ T2GE, HDCT	↑ T2, ↓ T2GE, HDCT	↓ T2	
3†	CECT		T1E, ↑ T2, ↓ T2GE	T1E, ↑ T2, ↓ T2GE, CECT	T1E, ↑ T2, CECT	T1E, ↑ T2
4	T1E, ↑ T2	T1E, ↑ T2	T1E, ↑ T2	T1E, ↑ T2	↑ T2	
5*	T1E, ↑ T2	T1E, ↑ T2	T1E, ↑ T2	T1E, ↑ T2	↑ T2	
6§	T1E, ↑ T2	T1E, ↑ T2	T1E, ↑ T2	T2FE	T2FE	

Note.—CECT indicates enhancement on contrast-enhanced CT images; HDCT, high attenuation (increased relative to gray matter) on nonenhanced CT images; T1E, enhancement on contrast-enhanced T1-weighted MR images, ↑ T1, increased signal intensity on T1-weighted MR images; T2FE, enhancement on T2 FLAIR sequence; ↑ T2, increased signal intensity on T2-weighted MR images; and ↓ T2GE, decreased signal on gradient-echo T2-weighted images.

* Other findings included phthisis bulbi.

† Other findings included T1E in the midbrain, superior cerebellar peduncle, temporal lobe and ↑ T2 in the thalamus, midbrain, pons, and cerebellum.

‡ Other findings included T1E in the midbrain and temporal lobe.

§ Other findings included T1E in the meninges, cerebellum, midbrain, Meckel cave and ↑ T2 and T2FE in the meninges, cerebellum, midbrain, and Meckel cave.

cerebellar artery, basilar artery, and other vessels in the circle of Willis have been shown to exist in animals (34). Resulting vasculitis with infarctions have been postulated to produce the MR imaging–detectable lesions reported in these cases.

Herpes viruses might conceivably disseminate through the CNS from the trigeminal nerve via trigeminal innervation of the meninges, with resultant CSF spread. HSV has been associated with viral meningitis and meningoencephalitis (35). HZV and HSV isolates have been detected in the CSF by means of immunoassay when remote dermatomal occurrence of infections have coincided with radiculopathy in the lumbar spine (30, 31, 36). However, animal studies testing this mode of spread were not found in the online literature.

In the four cases of HZV in our series, optic neuritis followed corneal disease by varying time intervals. In two cases, imaging findings could be traced to the lateral geniculate bodies. In one of these, the optic radiations and optic cortex were also involved. To spread from the optic tract to the optic radiation, the virus must cross the lateral geniculate synapses. One of three possible mechanisms can explain these phenomena: 1) the virus spreads trans-synaptically in these cases, 2) the virus spreads to the postganglionic neurons via the CSF or via the microvasculature, or 3) the virus “jumps” the synapses.

Our series is most consistent with transneuronal–trans-synaptic spread of HZV in most cases. However, some of our images are at least partially consistent with local meningeal spread via the CSF or microvasculature. Meningeal enhancement, including the involvement of the Meckel cave (patient 2, Fig 2; patient 6, Fig 5) and viral spread to the lateral brain stem (patient 3, Fig 3; patient 6, Fig 5), were observed. Furthermore, increased T2 signal intensity in the adjacent CSF was also observed on FLAIR images obtained in patient 6 (Fig 5).

Other findings, however, are difficult to explain with the meningeal–CSF mode of transmission. Con-

trast enhancement and increased T2 signal intensity were also seen in deep white matter and gray matter structures, which were remote from the CSF space in multiple cases. Furthermore, the pattern of spread was more closely related to the neuronal pathways than the vascular supply for most findings. The pattern of spread was conspicuously related to the visual pathways in most images, rather than the formation of a more geographic infection, as typically seen in bacterial infections and non–neuronally spread viral infections, such as progressive multifocal leukoencephalopathy. Additionally, autopsy results were available in one case and demonstrated zoster virus in the neuronal tissue. These findings support transneuronal spread of the virus, which is not surprising, given the accumulation of animal model and clinical data supporting this means of viral dissemination.

Further consideration can be given to the possibility of trans-synaptic spread. In patient 3 (Fig 3), the affected areas involved extensive regions remote from the initial site of infection and often involved tissues geographically related to the primary path of spread. It is reasonable to propose that the virus spread to these adjacent tissues through the interstitial tissues. If the virus can spread locally through the interstitium, there is little to prevent local trans-synaptic spread; the virus might then be further disseminated along axons in either antegrade or retrograde fashion.

Gliosis related to wallerian degeneration due to diseased retinal ganglion cells might conceivably account for the increased T2 signal intensity and atrophy that was correlated with the neuronal pathways. However, this possibility would not explain the contrast enhancement also observed at many of the same sites. Furthermore, increased signal intensity on non-enhanced T1-weighted images and high attenuation on CT scans were seen in some cases. These changes are typically secondary to hemorrhage or the deposition of divalent cations in association with inflammation or hemorrhage.

Conclusion

Our series clearly demonstrated imaging findings that indicate central inflammatory changes associated with ARN; these observations support the association of RBON-H with ARN. Our findings generally support CNS, as well as PNS, transneuronal and transsynaptic spread of the HZV and CMV in both immunodeficient patients and immunocompetent patients. Dissemination via CSF might also be contributory. Although local petechial hemorrhage and small-vessel vasculitis may contribute to the pathogenesis of the disease, our findings were poorly correlated with vasculitis and stroke involving the circle of Willis and other intermediate vessels, as other have proposed (32–34). The reported occurrence of RBON-H before ARN, together with our findings, could indicate a pathway in which HZV or CMV are transmitted first centrally (via fifth-nerve projections to the CNS vasculature or meninges) then peripherally to the retina (via the second nerve). We also observed inflammatory changes involving the superior colliculus, where the oculomotor nerves, fifth nerves and second nerves have synapses. This provides another pathway from the fifth to the second nerves, as well as a pathway to the extraocular muscles (via the third, fourth, and sixth nerves) from the sensory system. These interlinking connections have the potential to spread infection from the trigeminal ganglia to the extraocular muscles, sclera, and retina.

References

- Litoff D, Catalano RA. Herpes zoster optic neuritis in human immunodeficiency virus infection. *Arch Ophthalmol* 1990;108:782–783
- Selbst RG, Selhorst JB, Harbison JW, Myer EC. Parainfectious optic neuritis: report and review following varicella. *Arch Neurol* 1983;40:347–350
- Kuppermann BD, Quiceno JI, Wiley C, et al. Clinical and histopathologic study of varicella zoster virus retinitis in patients with the acquired immunodeficiency syndrome. *Am J Ophthalmol* 1994;188:589–600
- Mansour AM. Neuro-ophthalmic findings in acquired immunodeficiency syndrome. *J Clin Neuro-Ophthalmol* 1990;10:167–174
- Garweg J, Bohnke M. Varicella-zoster virus is strongly associated with atypical necrotizing herpetic retinopathies. *Clin Infect Dis* 1997;24:603–608
- Kashiwase M, Sata T, Yamauchi Y, et al. Progressive outer retinal necrosis caused by herpes simplex virus type 1 in a patient with acquired immunodeficiency syndrome. *Ophthalmology* 2000;107:790–794
- Deane JS, Bibby K. Bilateral optic neuritis following herpes zoster ophthalmicus. *Arch Ophthalmol* 1995;113:972–973
- Meenken C, van den Horm GJ, de Smet MD, van der Meer JT. Optic neuritis heralding varicella zoster virus retinitis in a patient with acquired immunodeficiency syndrome. *Ann Neurol* 1998;43:534–536
- Gunduz K, Ozdemir O. Bilateral retrobulbar neuritis following unilateral herpes zoster ophthalmicus. *Ophthalmologica* 1994;208:61–64
- Galindez OA, Sabates NR, Whittacre MM, Sabates FN. Rapidly progressive outer retinal necrosis caused by varicella zoster virus in a patient infected with human immunodeficiency virus. *Clin Infect Dis* 1996;22:149–151
- Margolis TP, Lowder CY, Holland GN, et al. Varicella zoster virus retinitis in patients with the acquired immunodeficiency syndrome. *Am J Ophthalmol* 1991;112:119–131
- Burke DG, Leonard DG, Imperiale TF, et al. The utility of clinical and radiographic features in the diagnosis of cytomegalovirus central nervous disease in AIDS patients. *Mol Diagn* 1999;4:37–43
- Eong KG, Beatty S, Charles SJ. Cytomegalovirus retinitis in patients with acquired immune deficiency syndrome. *Postgrad Med J* 1999;75:585–590
- Anonymous. Assessment of cytomegalovirus retinitis. Clinical evaluation vs centralized grading of fundus photographs: Studies of ocular complications of AIDS research group, AIDS clinical trials. *Arch Ophthalmol* 1996;114:791–805
- Flores-Aguilar M, Munguia D, Besen G, Gangan P, Arevalo JF, Freeman WR. Clinical versus fundus photographic evaluation of the status of cytomegalovirus retinitis in AIDS patients. *Retina* 1996;16:363–372
- Michalova K, Rihova E, Havlikova M. Acute retinal necrosis syndrome [Czech]. *Cesk Slov Oftalmol* 1996;52:319–324
- Ballinger R. CMV retinitis. *Optom Vis Sci* 1995;72:305–309
- Ormerod LD, Larkin JA, Margo CA, et al. Rapidly progressive herpetic retinal necrosis: a blinding disease characteristic of advanced AIDS. *Clin Infect Dis* 1998;26:34–45; discussion 46–47
- Pecorella I, Ciardi A, Credendino A, Marasco A, Di Tondo U, Scaravilli F. Ocular, cerebral and systemic interrelationships of cytomegalovirus infection in a post-mortem of AIDS patients. *Eye* 1999;13:781–785
- Batisse D, Eliaszewicz M, Zazoun L, et al. Acute retinal necrosis in the course of AIDS: study of 26 cases. *AIDS* 1996;10:55–60
- Friedlander JM, Rahdal FM, Ericson L, et al. Optic neuropathy preceding acute retinal necrosis in acquired immunodeficiency syndrome. *Arch Ophthalmol* 1996;114:1481–1485
- Fukutake T, Hatakeyama H, Shinotoh H, Hattori T. Herpes zoster ophthalmicus and delayed contralateral hemiparesis: a case of ipsilateral midbrain involvement. *Eur Neurol* 1998;40:57–58
- Cadavid D, Pearl PL, Dubovsky EC, Angiolillo A, Vezina LG. Stroke after zoster ophthalmicus in a 12-year-old girl with protein C deficiency. *Neurology* 1999;53:1128–1129
- Cavaletti G, Bogliun G, Tagliabue M. MRI evaluation of a case of herpes zoster ophthalmicus with delayed contralateral hemiplegia. *Ital J Neurol Sci* 1990;11:297–300
- Norgren RB Jr, McLean JH, Bubel HC, Wander A, Bernstein DI, Lehman MN. Anterograde transport of HSV-1 and HSV-2 in the visual system. *Brain Res Bull* 1992;28:393–399
- Sur JH, Kim SB, Osorio FA, Moon OK. Study of transneuronal passage of pseudorabies virus in rat central nervous system by use of immunohistochemistry and in situ hybridization. *Am J Vet Res* 1995;56:1195–2034
- Oliver KR; Fazakerley JK. Transneuronal spread of Semliki Forest virus in the developing mouse olfactory system is determined by neuronal maturity. *Neuroscience* 1998;82:867–877
- Schmidbauer M, Budka H, Pilz P, Kurata T, Hondo R. Presence, distribution and spread of productive varicella zoster virus infection in nervous tissues. *Brain* 1992;115:383–398
- Sartoretti-Schefer S, Kollias S, Valavanis A. Ramsay Hunt syndrome associated with brain stem enhancement. *AJNR Am J Neuroradiol* 1999;20:278–280
- Schoenhuber R, Bortolotti P, Panzetti P, Guerzoni MC, Colombo A. Lumbosacral herpes zoster myelitis. *Ital J Neurol Sci* 1986;7:541–543
- Nagane Y, Utsugisawa K, Yonezawa H, Tohgi H. A case with trigeminal herpes zoster manifesting a long lesion of the spinal trigeminal nucleus and tract on MR T2-weighted image. *Rinsho Shinkeigaku* 2001;41:56–59
- Hilt DC, Buchholz D, Krumholz A, Weiss H, Wolinsky JS. Herpes zoster ophthalmicus and delayed contralateral hemiparesis caused by cerebral angitis: diagnosis and management approaches. *Ann Neurol* 1983;14:543–553
- Melanson M, Chalk C, Georgevich L, et al. Varicella-zoster virus DNA in CSF and arteries in delayed contralateral hemiplegia: evidence for invasion of cerebral arteries. *Neurology* 1996;46:569–570
- Saito K, Moskowitz MA. Contributions from the upper cervical dorsal roots and trigeminal ganglia to the feline circle of Willis. *Stroke* 1989;20:524–526
- Ratzan KR. Viral meningitis. *Med Clin North Am* 1985;69:399–413
- Haanpaa M, Dastidar P, Weinberg A, et al. CSF and MRI findings in patients with acute herpes zoster. *Neurology* 1998;51:1405–1411